Semimicroscopic modeling of heavy-ion fusion reactions with multireference covariant density functional theory

K. Hagino[1,2,3] and J. M. Yao[1,4]

[1]*Department of Physics, Tohoku University, Sendai 980-8578, Japan*

[2]*Research Center for Electron Photon Science, Tohoku University, 1-2-1 Mikamine, Sendai 982-0826, Japan*

[3]*National Astronomical Observatory of Japan, 2-21-1 Osawa, Mitaka, Tokyo 181-8588, Japan*

[4]*School of Physical Science and Technology, Southwest University, Chongqing 400715, China*

(Received 15 April 2015; revised manuscript received 20 May 2015; published 9 June 2015)

We describe low-lying collective excitations of atomic nuclei with the multireference covariant density functional theory and combine them with coupled-channels calculations for heavy-ion fusion reactions at energies around the Coulomb barrier. To this end, we use the calculated transition strengths among several collective states as inputs to the coupled-channels calculations. This approach provides a natural way to describe anharmonic multiphonon excitations, as well as a deviation of rotational excitations from a simple rigid rotor. We apply this method to subbarrier fusion reactions of ^{58}Ni + ^{58}Ni, ^{58}Ni + ^{60}Ni, and ^{40}Ca + ^{58}Ni systems. We find that the effect of anharmonicity tends to smear the fusion barrier distributions, better reproducing the experimental data compared to the calculations in the harmonic oscillator limit.

DOI: 10.1103/PhysRevC.91.064606 PACS number(s): 25.70.Jj, 24.10.Eq, 21.60.Jz, 23.20.−g

I. INTRODUCTION

In heavy-ion fusion reactions at energies around the Coulomb barrier, low-lying collective excitations of the colliding nuclei during the fusion process play an important role in enhancing fusion cross sections as compared to a prediction of a simple potential model [1–3]. These effects have usually been taken into account in the coupled-channels calculations with a coupling scheme based on a harmonic vibrator for spherical nuclei or on a rigid rotor for deformed nuclei [4,5]. With this approach, the energy of the first excited state as well as the coupling strength from the ground state to the first excited state, which can be taken from the experimental data, specify all the other excitation energies and coupling strengths for higher members in the coupling scheme. Typical examples which show the subbarrier enhancement of fusion cross sections include the fusion of ^{58}Ni + ^{60}Ni and ^{64}Ni + ^{64}Ni, for which multiphonon excitations have been shown to play an important role [6,7]. See also Refs. [8,9] for discussions on multiphonon excitations. Multiple excitations within the ground-state rotational band also play an important role in most of fusion reactions involved with heavy deformed nuclei [10].

In reality, however, most atomic nuclei have neither a pure harmonic oscillator spectrum nor a pure rigid body rotational band. For example, the ^{58}Ni nucleus, which has usually been considered to be a typical vibrational nucleus, does not exhibit a level spectrum characteristic to the harmonic vibration; that is, the degeneracy of the two-phonon triplet is considerably broken. Moreover, a recent theoretical calculation based on a multireference density functional theory with the Skyrme interaction also indicates that the $B(E2)$ strengths among the collective levels in ^{58}Ni deviate largely from what are expected from a simple harmonic oscillator [11]. It is therefore of considerable interest to investigate the role of anharmonicity, that is, the deviation from the harmonic limit, in subbarrier fusion of ^{58}Ni.

In Refs. [12,13], the effect of anharmonicity on subbarrier fusion of ^{16}O + ^{144,148}Sm has been investigated using the vibrational limit of interacting boson model (IBM). See also Ref. [14] for an application of this method to large-angle quasielastic scattering of the ^{16}O + ^{144}Sm system. Although the static quadrupole moment of the first excited state could be successfully extracted by analyzing the high-precision experimental data with this approach [12,13], the application of IBM has several limitations for a global study. First, the method is not applicable to doubly magic nuclei, as the number of bosons in IBM is estimated from the number of valence nucleons outside shell closures. Second, phenomenological parameters have to be introduced to the model Hamiltonian and to the transition operators. It is therefore desirable to develop an alternative microscopic approach for nuclear collective excitations, which does not rely on the harmonic limit or the rigid rotor, to systematically investigate the effect of collective excitations in general on subbarrier fusion reactions in a wide mass region.

In this paper, we employ a beyond-mean-field method to describe low-lying collective excitations and combine it with the coupled-channels approach to heavy-ion fusion reactions. The pure mean-field approximation breaks the rotational symmetry and does not yield a spectrum of nuclei. This can be overcome by going beyond the mean-field approximation, in particular, by carrying out the angular-momentum projection. One can also take into account the quantum fluctuation of the mean-field wave function by superposing many Slater determinants with the generator coordinate method (GCM). When the pairing correlation is important, the particle-number projection can also be implemented. Such a scheme has been referred to as a multireference density-functional theory (MR-DFT) and has rapidly been developed in nuclear-structure physics for the past decade [15,16].

The paper is organized as follows. In Sec. II, we briefly review the coupled-channels approach for heavy-ion subbarrier fusion reactions. In Sec. III, we present the results of MR-DFT calculations for the ^{58}Ni and ^{60}Ni nuclei. To this end, we use the covariant density functional theory (CDFT), based on the relativistic framework. In Sec. IV, we combine the

coupled-channels calculations with the MR-CDFT approach. We apply this method to subbarrier fusion reactions of ^{58}Ni + ^{58}Ni, ^{58}Ni + ^{60}Ni, and ^{40}Ca + ^{58}Ni systems and discuss the role of anharmonicity of quadrupole vibrations of ^{58}Ni and ^{60}Ni. We then summarize the paper in Sec. V.

II. COUPLED-CHANNELS APPROACH TO HEAVY-ION FUSION REACTIONS

Our aim in this paper is to solve coupled-channels equations using inputs from the MR-CDFT calculations. In principle, one could formulate the coupled-channels method fully microscopically using the MR-CDFT method. In such an approach, the internuclear potentials, both for the diagonal and the coupling parts, would be constructed by folding an effective nucleon-nucleon interaction with calculated density distributions and transition densities [17]. It has been known, however, that this double folding procedure fails to work for heavy-ion subbarrier fusion reactions [5]. That is, one obtains a surface diffuseness parameter of around $a \sim 0.63$ fm when a double folding potential is fitted with a Woods-Saxon function, whereas experimental fusion cross sections systematically require a much larger value, e.g., $a \sim 1.0$ fm [10,18–22]. An important fact to notice is that the double folding method works only in the surface region of the potential. For elastic and inelastic scattering, the surface region of the potential is mainly probed and a double folding potential is reasonable [22–26]. In marked contrast, fusion reactions involve both the surface and the inner regions, where two nuclei appreciably overlap with each other. As a consequence, several dynamical effects are important in the inner region [27–31], and the double folding potential looses its validity.

Another problem of the fully microscopic formulation is that the MR-CDFT calculations seldom yield a perfect agreement with experimental data for excitation energies and transition strengths, even though an overall agreement is often reasonable. However, to describe quantitatively heavy-ion fusion reactions at energies close to the Coulomb barrier, it is important to use reasonable values for excitation energies and transition strengths.

To avoid these drawbacks of the fully microscopic approach, in this paper we employ a semimicroscopic approach. That is, we use a phenomenological Woods-Saxon internuclear potential and adopt the experimental value for the coupling strength between the ground state and the first excited state. The coupling strengths for higher members are not known well in many nuclei, and it is for these values that we employ the MR-CDFT calculations, after scaling the calculated values with the experimental strength for the transition between the ground state and the first excited state. The excitation energies are known for most of the collective levels, and we simply use the experimental values whenever they are available.

In the coupled-channels approach to subbarrier fusion reactions, one expands the total wave function of the system in terms of the eigenfunctions of the collective states in the target nucleus, $|\varphi_{J0}\rangle$, as

$$\Psi_{LM_L}(\boldsymbol{r}) = \sum_J \frac{u_J(r)}{r} Y_{LM_L}(\hat{\boldsymbol{r}})|\varphi_{J0}\rangle, \tag{1}$$

where r is the relative coordinate between the colliding nuclei and J and L are the angular momentum for the target state and the angular momentum for the relative motion, respectively. Here, for simplicity of notation, we have assumed that the projectile nucleus is inert, but an extension is straightforward to the case where both the projectile and the target nuclei are excited. We have also introduced the isocentrifugal approximation [5] and have assumed that the angular momentum for the relative motion does not change by the excitation of the target nucleus. Notice that only the $J_z = 0$ component is excited in the target nucleus in the isocentrifugal approximation.

Substituting Eq. (1) to the projected Schrödinger equation for the energy E, that is, $\langle\varphi_{J0}|H - E|\Psi_{LM_L}\rangle = 0$, where H is the total Hamiltonian, one obtains the coupled-channels equations for the radial wave functions $u_J(r)$ as [5]

$$\left[-\frac{\hbar^2}{2\mu}\frac{d^2}{dr^2} + \frac{L(L+1)\hbar^2}{2\mu r^2} + V_0(r) - E + \epsilon_J\right]u_J(r) + \sum_{J'} V_{JJ'}(r)u_{J'}(r) = 0, \tag{2}$$

where μ is the reduced mass for the relative motion, $V_0(r)$ is the bare potential, and ϵ_J is the energy of the target state J. $V_{JJ'}(r)$ are the coupling matrix elements given by

$$V_{JJ'}(r) = \langle\varphi_{J0}|V_{\rm coup}(r,\alpha_{\lambda 0})|\varphi_{J'0}\rangle, \tag{3}$$

where $V_{\rm coup}$ is the coupling potential and $\alpha_{\lambda 0}$ is the excitation operator with a multipolarity λ. We solve the coupled-channels equations by imposing the incoming wave boundary condition at $r = r_{\rm abs}$ inside the Coulomb barrier [5]; that is,

$$u_J(r) \sim \sqrt{\frac{k_{J_0}}{k_J(r)}}\mathcal{T}^L_{JJ_0}\exp\left[-i\int_{r_{\rm abs}}^{r} k_J(r')dr'\right] \quad (r \leqslant r_{\rm abs}) \tag{4}$$

$$= H_L^{(-)}(k_J r)\delta_{J,J_0} - \sqrt{\frac{k_{J_0}}{k_J}}\mathcal{S}^J_{JJ_0}H_L^{(+)}(k_J r) \quad (r \to \infty), \tag{5}$$

where $H_L^{(+)}$ and $H_L^{(-)}$ are the outgoing and the incoming Coulomb wave functions, respectively. $\mathcal{S}^L_{JJ_0}$ and $\mathcal{T}^L_{JJ_0}$ are the nuclear S matrix and the transmission coefficient, respectively, with $J_0 = 0$ being the spin of the ground state of the target nucleus. $k_J(r)$ is the local wave number given by

$$k_J(r) = \sqrt{\frac{2\mu}{\hbar^2}\left[E - \epsilon_J - \frac{L(L+1)\hbar^2}{2\mu r^2} - V_0(r)\right]}, \tag{6}$$

whereas $k_J = k_J(r = \infty) = \sqrt{2\mu(E - \epsilon_J)/\hbar^2}$. The fusion cross section $\sigma_{\rm fus}$ is then obtained as

$$\sigma_{\rm fus}(E) = \frac{\pi}{k^2}\sum_L (2L+1)P_L(E), \tag{7}$$

with $P_L(E) = \sum_J |\mathcal{T}^L_{JJ_0}|^2$.

As we have mentioned, we employ the Woods-Saxon potential for the nuclear part of the bare potential, $V_0^{(N)}(r)$; that is,

$$V_0^{(N)}(r) = -\frac{V_0}{1 + \exp[(r - R_0)/a]}. \tag{8}$$

The nuclear coupling potential is obtained by deforming the radius R_0 to

$$R_0 \to R_0 + R_T \sum_\mu \alpha_{\lambda\mu} Y^*_{\lambda\mu}(\hat{\boldsymbol{r}}), \tag{9}$$

where R_T is the radius of the target nucleus. Here the deformation parameter $\alpha_{\lambda\mu}$ is related to the electric multipole operator as [32]

$$Q_{\lambda\mu} = \frac{3e}{4\pi} Z_T R_T^2 \alpha_{\lambda\mu}, \tag{10}$$

where Z_T is the atomic number of the target nucleus. The coupling potential in Eq. (3) in the isocentrifugal approximation then reads [5]

$$\begin{aligned} V_{\rm coup}(r,\alpha_{\lambda 0}) = &-\frac{V_0}{1+\exp\left[\left(r - R_0 - \sqrt{\frac{2\lambda+1}{4\pi}} R_T \alpha_{\lambda 0}\right)/a\right]} \\ &+ \frac{3}{2\lambda+1} Z_P Z_T e^2 \frac{R_T^\lambda}{r^{\lambda+1}} \sqrt{\frac{2\lambda+1}{4\pi}} \alpha_{\lambda 0} \\ &- V_0^{(N)}(r), \end{aligned} \tag{11}$$

where we have also included the Coulomb coupling potential. The last term is to avoid the double counting in Eq. (2).

The matrix elements of $V_{\rm coup}$, Eq. (3), can be evaluated with the method employed in the computer code CCFULL [4,5]. To this end, one needs the matrix elements of the operator $\sqrt{\frac{2\lambda+1}{4\pi}}\alpha_{\lambda 0}$. In the following, we define the coupling strengths for the coupled-channels calculations as

$$\frac{\beta^{(\lambda)}_{JJ'}}{\sqrt{4\pi}} \equiv \sqrt{\frac{2\lambda+1}{4\pi}} \langle \varphi_{J0} | \alpha_{\lambda 0} | \varphi_{J'0} \rangle. \tag{12}$$

For the quadrupole harmonic oscillator with $\lambda = 2$, this definition yields [5]

$$\beta^{(\lambda=2)}_{J2_1} = \sqrt{2}\, \beta^{(\lambda=2)}_{2_1 0_1} \langle 2020 | J0 \rangle, \tag{13}$$

for the coupling between the one-phonon state (that is, the 2^+_1 state) to the two-phonon state with the angular momentum J. Notice that $\sqrt{\sum_{J=0,2,4} (\beta^{(\lambda=2)}_{J2_1})^2} = \sqrt{2}\, \beta^{(\lambda=2)}_{2_1 0_1}$, which has often been employed in the coupled-channels calculations with multiphonon couplings [4,5,7–9]. For a rigid rotor, one obtains

$$\beta^{(\lambda=2)}_{22} = \frac{2\sqrt{5}}{7}\beta, \quad \beta^{(\lambda=2)}_{24} = \frac{6}{7}\beta, \quad \beta^{(\lambda=2)}_{44} = \frac{20\sqrt{5}}{77}\beta, \tag{14}$$

with $\beta^{(\lambda=2)}_{20} \equiv \beta$ (see Eq. (3.49) in Ref. [5]).

With microscopic nuclear-structure calculations, the coupling strengths can be estimated as [see Eqs. (10) and (12)],

$$\frac{\beta^{(\lambda)}_{JJ'}}{\sqrt{4\pi}} = \sqrt{\frac{2\lambda+1}{4\pi}} \frac{4\pi}{3 Z_T e R_T^2} \langle \varphi_{J0} | Q_{\lambda 0} | \varphi_{J'0} \rangle, \tag{15}$$

where the quantity $\langle \varphi_{J0} | Q_{\lambda 0} | \varphi_{J'0} \rangle$ can be evaluated microscopically using the operator $Q_{\lambda\mu} = \sum_i r_i^\lambda Y_{\lambda\mu}(\hat{\boldsymbol{r}}_i)$.

In coupled-channels calculations for heavy-ion reactions, one sometimes uses a different value of the nuclear coupling strength from the Coulomb coupling strength; see, e.g., Ref. [7]. While the Coulomb coupling strength, β_C, can be estimated from a measured electric transition strength, $B(E\lambda)$, the nuclear coupling strengths, β_N, are taken rather arbitrarily. One of the big advantages of the semimicroscopic approach is that the nuclear coupling strengths can also be estimated by using the isoscalar operator for $Q_{\lambda\mu}$; that is,

$$Q^{(\rm IS)}_{\lambda\mu} = \sum_{i\in p,n} r_i^\lambda Y_{\lambda\mu}(\hat{\boldsymbol{r}}_i) = \frac{3}{4\pi} A_T R_T^2 \alpha_{\lambda\mu}, \tag{16}$$

whereas the Coulomb coupling strengths are related to the $E\lambda$ operator,

$$Q^{(\rm E\lambda)}_{\lambda\mu} = e \sum_{i\in p} r_i^\lambda Y_{\lambda\mu}(\hat{\boldsymbol{r}}_i) = \frac{3e}{4\pi} Z_T R_T^2 \alpha_{\lambda\mu}. \tag{17}$$

From these equations, one obtains

$$\frac{\beta_N}{\beta_C} = \frac{Z_T}{A_T}\left(1 + \frac{M_n}{M_p}\right), \tag{18}$$

where M_n/M_p is the neutron-to-proton ratio for a transition given by

$$\frac{M_n}{M_p} = \frac{\langle \varphi_{JM} | \sum_{i\in n} r_i^\lambda Y_{\lambda\mu}(\hat{\boldsymbol{r}}_i) | \varphi_{J'M'} \rangle}{\langle \varphi_{JM} | \sum_{i\in p} r_i^\lambda Y_{\lambda\mu}(\hat{\boldsymbol{r}}_i) | \varphi_{J'M'} \rangle}. \tag{19}$$

Notice that for a pure isoscalar transition, M_n/M_p is reduced to N_T/Z_T, and the nuclear and the Coulomb coupling strengths are identical to each other; that is, $\beta_N = \beta_C$.

III. MULTIREFERENCE COVARIANT DENSITY FUNCTIONAL CALCULATION FOR ^{58}Ni AND ^{60}Ni

Let us now carry out the MR-CDFT calculations for the ^{58}Ni and ^{60}Ni nuclei and obtain inputs for the coupled-channels calculations. These nuclei have been studied recently in Ref. [11] using the nonrelativistic MR-DFT method. Here we repeat similar calculations with the relativistic framework to check the dependence of the conclusions on a choice of energy density functional.

In the MR-CDFT [16,33–35], the wave function for nuclear low-lying states is constructed as a superposition of projected mean-field states corresponding to a different deformation parameter β,

$$|\alpha J M; N Z\rangle = \sum_\beta f^J_\alpha(\beta) \hat{P}^J_{M0} \hat{P}^N \hat{P}^Z |\Phi(\beta)\rangle, \tag{20}$$

where $\alpha = 1,2,\ldots$ distinguishes different collective states with the same angular momentum J. Here $|\Phi(\beta)\rangle$ are the mean-field states generated by the deformation-constrained relativistic mean-field (RMF) method. The pairing correlation is taken into account in the BCS approximation. For simplicity, we have assumed the axial and reflection symmetries for the mean-field states. Thus, the K quantum number (that is, the projection of angular momentum onto the z axis) is zero, and the index K has been dropped. We implement both the particle-number and the angular-momentum projections. The projection operators $\hat{P}^N$, $\hat{P}^Z$, and $\hat{P}^J$ in Eq. (20) project the mean-field states onto the states with good neutron and proton numbers N, Z, as well as a good angular momentum J.

The weight coefficients $f_\alpha^J(\beta)$ in Eq. (20) are determined by solving the Hill-Wheeler-Griffin (HWG) equations [32],

$$\sum_{\beta'}\left[\mathcal{H}_{00}^J(\beta,\beta') - E_\alpha^J \mathcal{N}_{00}^J(\beta,\beta')\right] f_\alpha^J(\beta') = 0, \qquad (21)$$

where $\mathcal{N}_{00}^J(\beta,\beta')=\langle\Phi(\beta)|\hat{P}_{00}^J\hat{P}^N\hat{P}^Z|\Phi(\beta')\rangle$ and $\mathcal{H}_{00}^J(\beta,\beta') = \langle\Phi(\beta)|\hat{H}\hat{P}_{00}^J\hat{P}^N\hat{P}^Z|\Phi(\beta')\rangle$ are the norm and the energy kernels, respectively. The prescription of mixed density is adopted for the energy kernel. The detailed expressions for the kernels can be found in Refs. [16,33–35]. The solution of the HWG equation provides the energy levels and the information on the matrix elements $\langle\varphi_{J0}|Q_{\lambda 0}|\varphi_{J'0}\rangle$ in Eq.(15) with $|\varphi_{JM}\rangle = |\alpha JM;NZ\rangle$, which are needed for the coupled-channels calculations for fusion cross sections. Notice that in most cases it is hard to determine experimentally the sign of this matrix element even if information is sometimes available on its absolute value from the electric transition probabilities [7] (see also Ref. [36]). An advantage of the present semimicroscopic approach is that the matrix elements can be estimated theoretically, including their sign as well.

Figure 1(a) shows the energy curves of particle-number and angular-momentum-projected states with $J = 0$, 2, 4, and 6 for ^{58}Ni as a function of the intrinsic mass quadrupole deformation β of the mean-field states. The PC-PK1 parameter set [37] is used for the nucleon-nucleon interaction. The figure also shows the low-lying collective states obtained by mixing the symmetry conserved states. These states are plotted at their

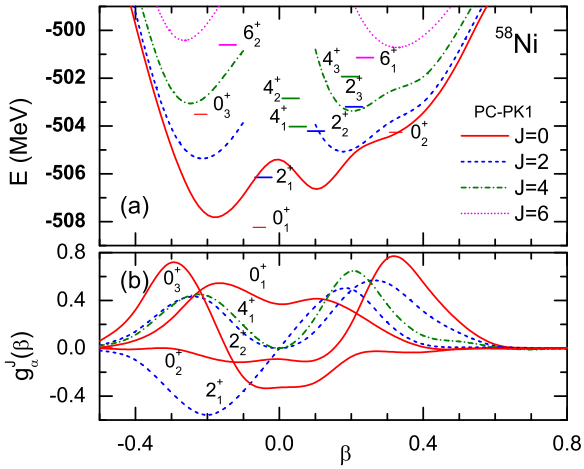

FIG. 1. (Color online) (a) The total energy for the angular-momentum-projected states with $J = 0$, 2, 4, and 6 for ^{58}Ni as a function of the intrinsic mass quadrupole deformation β of the mean-field states. The particle-number projection has also been implemented. Those curves are obtained with the projected CDFT method with PC-PK1 interaction [37]. The low-lying collective levels, obtained with the configuration mixing calculation, are also plotted at their average deformation $\bar{\beta}$. (b) The collective wave functions given by Eq. (23) for the states indicated in the figure as a function of deformation parameter β.

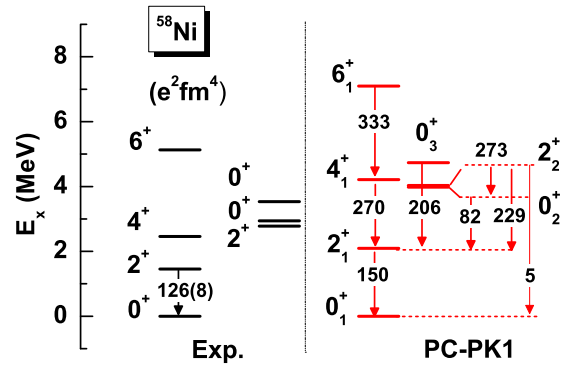

FIG. 2. (Color online) Comparison of the experimental and the calculated low-lying energy spectra of ^{58}Ni. The experimental data are taken from Refs. [38,39], while the calculated spectrum is obtained with the PC-PK1 force. The $E2$ transition strengths are given in units of e^2 fm^4.

average deformation $\bar{\beta}$ defined as

$$\bar{\beta}(J_\alpha) = \sum_\beta \beta\left|g_\alpha^J(\beta)\right|^2, \qquad (22)$$

where the collective wave functions $g_\alpha^J(\beta)$ are related to the weight functions in Eq. (20) as

$$g_\alpha^J(\beta) = \sum_{\beta'}\left[\mathcal{N}_{00}^J\right]^{1/2}(\beta,\beta') f_\alpha^J(\beta'). \qquad (23)$$

These collective wave functions are plotted in Fig. 1(b).

To facilitate the discussion on the properties of these states, we collect them and make a comparison with the experimental spectrum in Fig. 2. The results for the ^{60}Ni are also shown in Fig. 3. One can see that the main feature of the energy spectrum and the $E2$ transition strength from 2_1^+ to 0_1^+ are reproduced rather well. These results are qualitatively similar to the results of the previous MR-DFT calculations with the nonrelativistic Skyrme SLy4 interaction [11], but quantitatively the present calculations with the relativistic DFT reproduce the experimental data slightly better. For instance, the $B(E2)$ value from the 2_1^+ to the 0_1^+ states in ^{58}Ni was 248 e^2 fm^4 in the previous calculation [11], while it is 150 e^2 fm^4 in the present calculation, which is much closer to the experimental value of 126(8) e^2 fm^4 [38,39].

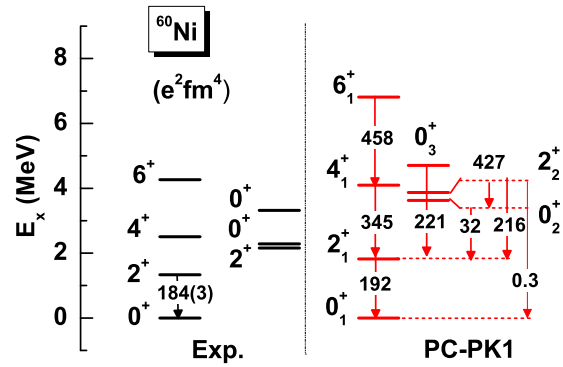

FIG. 3. (Color online) Same as Fig. 2, but for ^{60}Ni.

It is interesting to notice that the overall pattern of $B(E2)$ values is quite different from what would be expected for a harmonic vibrator, even though the excitation energies of the 4_1^+, 2_2^+, and 0_2^+ states are about twice the energy of the 2_1^+ state. In particular, the $E2$ transition from the 0_2^+ to the 2_1^+ states is much smaller than that from the 4_1^+ and the 2_2^+ states to the 2_1^+ state, which is similar to Cd isotopes [40,41]. Instead, the 0_2^+ state has a strong transition from the 2_2^+ state, which clearly indicates that the 0_2^+ state is not a member of the two-phonon triplet. Notice that the collective wave function for each of the 4_1^+ and 2_2^+ states have a similar structure to one another [see Fig. 1(b)]. However, the 0_2^+ state has a considerably different wave function from those states, being dominated by the mean-field configurations around $\beta = 0.3$.

Compared to the 0_2^+ state, the $E2$ transition strength from the 0_3^+ to the 2_1^+ states is much larger and is comparable to that from the 4_1^+ and the 2_2^+ states to the 2_1^+ state. This fact makes the 0_3^+ state a better candidate for a member of the two-phonon triplets, even though the excitation energy is a little bit large and its collective wave function is much different from that for the 4_1^+ and the 2_2^+ states. A similar conclusion has been reached also with the nonrelativistic DFT [11].

Notice that, in the harmonic oscillator limit, the $B(E2)$ value from any of the two-phonon triplet states to the 2_1^+ state is exactly twice the $B(E2)$ value from the 2_1^+ state to the ground state [42]. The calculated $B(E2)$ values shown in Figs. 2 and 3, together with the strong transition from the 2_2^+ to the 0_2^+ states, indicate a presence of large anharmonicity in the quadrupole vibrations in ^{58}Ni and ^{60}Ni. That is, the calculated $B(E2)$ values are significantly quenched from the values in the harmonic limit. This fact also implies that the present approach for fusion reactions with MR-CDFT provides a natural truncation scheme in the coupled-channels calculations, whereas the truncation of the phonon spectrum has to be introduced in an *ad hoc* way if one employs the harmonic oscillator couplings.

Another clear indication of anharmonicity is a finite value of quadrupole moment of the first 2^+ state. Experimentally, the spectroscopic quadrupole moment of the first 2^+ state has been measured to be $Q(2_1^+) = -10 \pm 6\ e\,\mathrm{fm}^2$ for ^{58}Ni and $Q(2_1^+) = +3 \pm 5\ e\,\mathrm{fm}^2$ for ^{60}Ni [43]. The present MR-CDFT calculations yield $Q(2_1^+) = +7.96$ and $+10.4\ e\,\mathrm{fm}^2$ for ^{58}Ni and ^{60}Ni, respectively. Even though the sign of quadrupole moment is opposite that of the experimental data for ^{58}Ni, the MR-CDFT calculations predict a similar absolute value of quadrupole moment to the experimental value both for ^{58}Ni and ^{60}Ni. Notice that the average deformation for the 2_1^+ state is very small for both of these nuclei owing to a large cancellation between the prolate and the oblate components, as shown in Fig. 1. A more careful numerical treatment of the calculations would therefore be necessary to reproduce the correct sign of the quadrupole moment, although it is beyond the scope of the present paper.

IV. FUSION OF Ni ISOTOPES

In the previous section, we have seen that both ^{58}Ni and ^{60}Ni do not show a typical behavior of harmonic oscillator. Let us now investigate how the deviation of the spectrum from the harmonic limit affects the subbarrier fusion reactions of Ni isotopes.

We first consider the fusion reaction of two ^{58}Ni nuclei. Because we assume the axial and reflection symmetries in the present MR-CDFT calculations, at this moment we are unable to describe both the octupole vibration, 3^-, and the 3^+ state in the three-phonon multiplets. We therefore consider only the quadrupole two-phonon excitations in each ^{58}Ni nucleus. Table I summarizes the coupling strengths, obtained with the MR-CDFT calculation discussed in the previous section [see Eq. (15)]. We use $R_T = 1.06 \times 58^{1/3}$ fm for the radius of ^{58}Ni. The phase of each of the collective wave functions is chosen so that the sign of the off-diagonal components is identical to that in the harmonic oscillator limit. The Coulomb coupling strength for the transition between the ground state and the first 2^+ state is estimated to be $\beta = 0.223$ using the measured

TABLE I. The Coulomb coupling strengths for the quadrupole transitions in ^{58}Ni, estimated with the microscopic MR-CDFT calculations with PC-PK1 force [see Eq. (15)]. The values in the parentheses are the corresponding nuclear coupling strengths obtained with Eq. (18). The radius parameter of $r_0 = 1.06$ fm is used, and the calculated values are scaled with the Coulomb coupling strength for the transition from the ground state to the first 2^+ state, which is estimated with the measured $B(E2)$ value.

	I'					
I	0_1^+	2_1^+	0_2^+	2_2^+	4_1^+	0_3^+
0_1^+	0	0.223 (0.245)	0	0.0390 (0.0228)	0	0
2_1^+	0.223 (0.245)	−0.0457 (−0.0311)	0.0736 (0.0668)	−0.147 (−0.155)	0.215 (0.229)	0.117 (0.108)
0_2^+	0	0.0736 (0.0668)	0	−0.300 (−0.278)	0	0
2_2^+	0.0390 (0.0228)	−0.147 (−0.155)	−0.300 (−0.278)	0.0873 (0.0777)	−0.0617 (−0.0610)	0.165 (0.170)
4_1^+	0	0.215 (0.229)	0	−0.0617 (−0.0610)	0.0279 (0.0405)	0
0_3^+	0	0.117 (0.108)	0	0.165 (0.170)	0	0

TABLE II. The strengths for the Coulomb coupling in ^{58}Ni in the harmonic oscillator limit. Here we have assumed that the third 0^+ state belongs to the two-phonon triplet.

	I'					
I	0_1^+	2_1^+	0_2^+	2_2^+	4_1^+	0_3^+
0_1^+	0	0.223	0	0	0	0
2_1^+	0.223	0	0	−0.169	0.226	0.141
0_2^+	0	0	0	0	0	0
2_2^+	0	−0.169	0	0	0	0
4_1^+	0	0.226	0	0	0	0
0_3^+	0	0.141	0	0	0	0

$B(E2)$ value with the same radius parameter. The calculated values of the coupling strengths shown in Table I have been scaled to this value, which amounts to multiplying a factor of 0.916 to all the calculated coupling strengths. In Table I, the values in the parentheses are the nuclear coupling strengths, calculated with the theoretical value for M_n/M_p based on Eq. (18). For a comparison, we also show in Table II the Coulomb coupling strengths in the harmonic oscillator limit, assuming the third 0^+ state to be a member of the two-phonon triplet. As we have mentioned in the previous section, the coupling strengths in ^{58}Ni shown in Table I reveal some similarity to the harmonic oscillator. That is, the coupling strengths from the one-phonon state (the 2_1^+ state) to the two-phonon states (that is, the 2_2^+, 4_1^+, and 0_3^+ states) are close to those in the harmonic limit. However, there are also pronounced deviations from the harmonic limit as well. That is, the strong couplings are present between the 2_2^+ and the 0_2^+ states and also between the 0_3^+ and the 2_2^+ states. The latter is zero in the harmonic limit, and so is the former unless the 0_2^+ is a member of the three-phonon multiplets.

Figures 4(a) and 4(b) show the fusion cross section $\sigma_{\rm fus}(E)$ and the fusion barrier distribution $D_{\rm fus}(E)$ defined as [1,45]

$$D_{\rm fus}(E) = \frac{d^2(E\sigma_{\rm fus})}{dE^2} \tag{24}$$

for the ^{58}Ni + ^{58}Ni reaction, respectively. We use the Woods-Saxon potential with $V_0 = 170.2$ MeV, $r_0 = 1.0$ fm, and $a = 0.9$ fm, where the radius R_0 is given as $R_0 = r_0(A_T^{1/3} + A_T^{1/3})$. The fusion barrier distributions are obtained with the point difference formula with the energy step of $\Delta E_{\rm c.m.} = 2$ MeV to be consistent with the experimental barrier distribution extracted in Ref. [6]. The dashed line shows the result of the coupled-channels calculations including up to the double-phonon states in the harmonic oscillator limit. All the mutual excitations between the projectile and the target nuclei are included. However, the solid line in the figure is obtained with the coupling strengths shown in Table I. To this end, we include the 0_1^+, 2_1^+, 0_3^+, 2_2^+, and 4_1^+ states in the coupled-channels calculations. Again, all the mutual excitation channels are taken into account. We use the experimental excitation energies for these states; that is, $\epsilon = 0$, 1.454, 3.531, 2.775, and 2.459 MeV, respectively. For a comparison, the figure also shows the result of the no-coupling limit by the dotted line. One

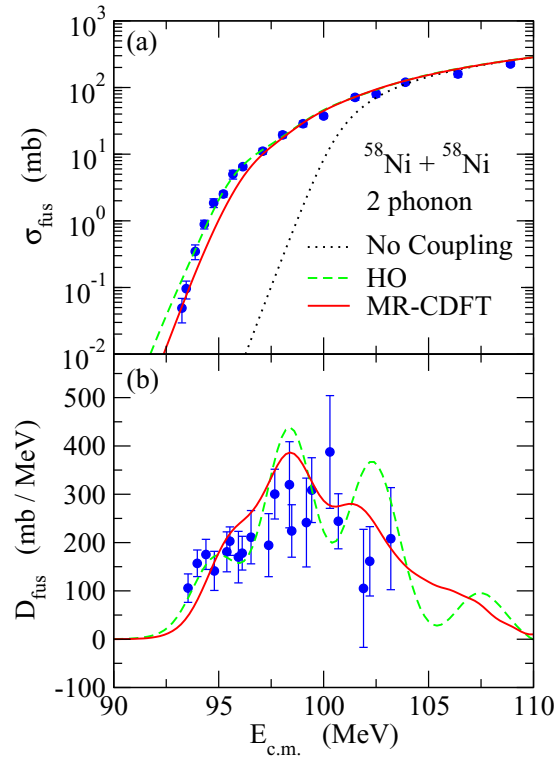

FIG. 4. (Color online) The fusion cross sections (a) and the fusion barrier distributions (b) for the ^{58}Ni + ^{58}Ni system. Here the fusion barrier distribution is defined as $D_{\rm fus}(E) = d^2(E\sigma_{\rm fus})/dE^2$. The dashed line is the result of the coupled-channels calculations, including the double quadrupole-phonon excitations in each ^{58}Ni nucleus in the harmonic oscillator limit, while the solid line is obtained by including the 0_1^+, 2_1^+, 0_3^+, 2_2^+, and 4_1^+ states with the coupling strengths shown in Table I. The dotted line denotes the result in the absence of the channel couplings. The experimental data are taken from Ref. [44] for the fusion cross sections and from Ref. [6] for the fusion barrier distribution.

can see that the calculations in the harmonic limit overestimate fusion cross sections at the two lowest energies, while the MR-CDFT calculations underpredict fusion cross sections around 95 MeV. However, for the energy dependence of fusion cross sections, shown in terms of fusion barrier distribution in panel (b) of the figure, the MR-CDFT calculation leads to a minor improvement by considerably smearing each peak.

As we have mentioned, to draw Fig. 4, we have multiplied a constant factor to the calculated transition strengths so that the transition rate from the first 2^+ state to the ground state coincides with the experimental data. We have also used the experimental values for the excitation energies. Figure 5(a) shows the fusion barrier distribution $D_{\rm fus}$ obtained without this prescription, that is, obtained by using the calculated transition strengths and excitation energies as they are. As shown in Fig. 2, the PC-PK1 interaction somewhat overestimates the energy of the first 2^+ state (2.09 MeV as compared to the experimental value of 1.45 MeV), although the $B(E2)$ strength is reproduced reasonably well; that is, $B(E2 : 2_1^+ \to 0_1^+) = 150.1\ e^2\ {\rm fm}^4$ as compared to the experimental value of 126(8) $e^2\ {\rm fm}^4$. Because the shape of fusion barrier distribution is

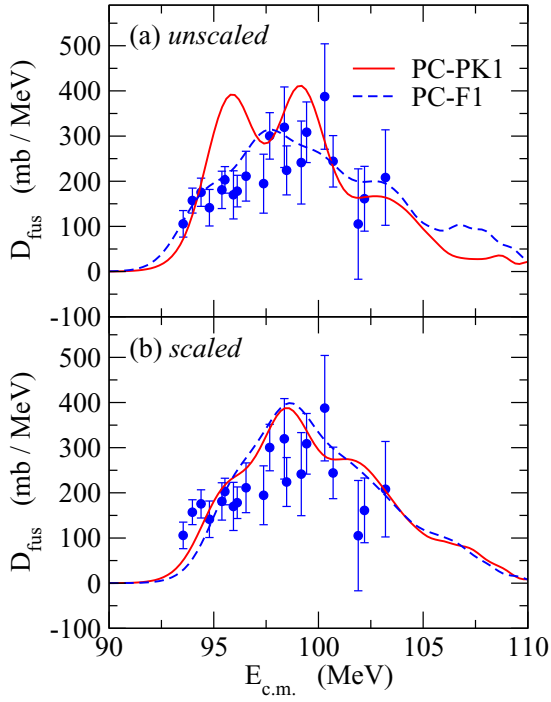

FIG. 5. (Color online) Comparison of the fusion barrier distribution for the ^{58}Ni + ^{58}Ni reaction obtained with several methods. (a) Results obtained with the calculated transition strengths and the excitation energies for the two-phonon couplings in ^{58}Ni. The solid and dashed lines show the results with the PC-PK1 and PC-F1 interactions, respectively. Panel (b) is obtained by using the experimental values for the excitation energies and also by multiplying a constant factor to the transition strengths so that the $B(E2)$ value from the first 2^+ state to the ground state coincides with the experimental value.

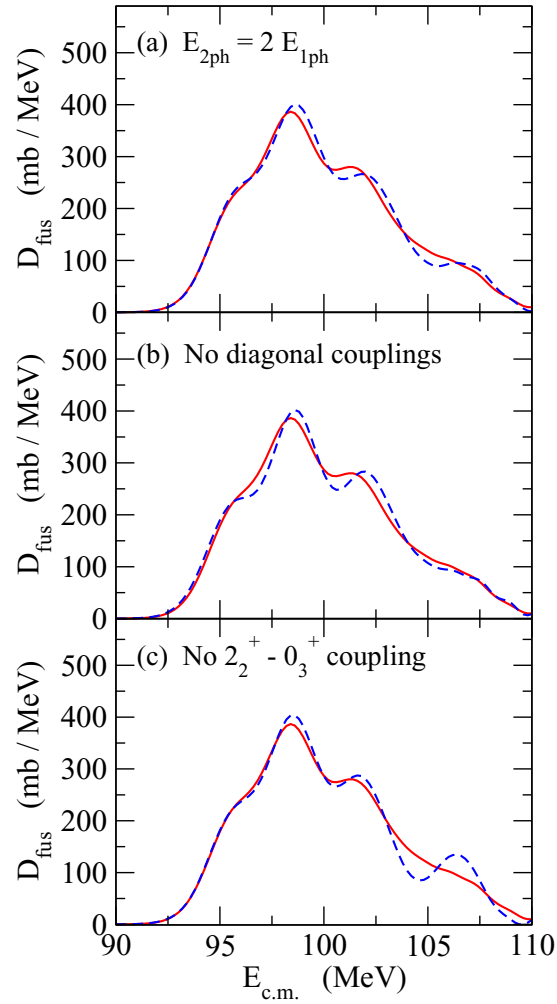

FIG. 6. (Color online) The fusion barrier distributions for the ^{58}Ni + ^{58}Ni reaction obtained with several coupling schemes. In all the panels, the solid line denotes the result of the MR-CDFT calculation shown in Fig. 4. In (a), the dashed line is obtained by setting the energy of the two-phonon triplet to be exactly twice the energy of the first 2^+ state. In (b), the dashed line is obtained by setting all the diagonal couplings to be zero, while in (c) it is obtained by setting the coupling strength to be zero for the transition from the second 2^+ state to the third 0^+ state.

sensitive to the energy of the first excited state [5], this calculation does not lead to a good reproduction of the experimental data, especially around $E_{\rm c.m.} = 95$ MeV. This implies that it is essential in the present approach to use the experimental values for the energy and the transition strength for the first 2^+ state to reproduce the experimental fusion barrier distribution.

For comparison, the figure also shows the results with the PC-F1 interaction [46] by the dashed line. This interaction yields the energy of the 2^+ state to be 1.58 MeV and thus reproduces the experimental energy much better than the PC-PK1 interaction. However, the transition strengths are largely overestimated; e.g., the calculated value for $B(E2 : 2_1^+ \rightarrow 0_1^+)$ is 199.1 e^2 fm^4. Even though this interaction well reproduces the experimental fusion barrier distribution even without the scaling, this might be accidental given that the transition strengths are incompatible with the experimental data. After scaling the transition strengths, the dependence of the results on the parameter set of the interaction becomes much weaker, as is shown in Fig. 5(b).

To understand the origins for the smearing in fusion barrier distribution owing to the anharmonicity effects, we repeat the same calculations as those shown in Fig. 4 with three different coupling schemes. In the first scheme, the energy of the two-phonon triplets is set to be exactly twice the energy of the first 2^+ state. The result for this is shown in Fig. 6(a). In the second scheme, all the diagonal couplings are set to be zero, while in the third scheme the coupling strength is set to be zero between the 2_2^+ and the 0_3^+ states. The results of these schemes are plotted in Figs. 6(b) and 6(c), respectively. One can see that all of these coupling schemes lead to a more structured barrier distribution than the full MR-CDFT calculations, and thus all of these three effects, together with the quenching of the coupling between the one-phonon and the two-phonon states, coherently contribute to the smearing in the barrier distribution. Among them, the effect shown in Fig. 6(c) seems to yield the largest effect.

In connection to Fig. 6(b), Fig. 7 shows the sensitivity of the fusion cross section and the fusion barrier distribution to the sign of quadrupole moment of the first 2^+ state. The

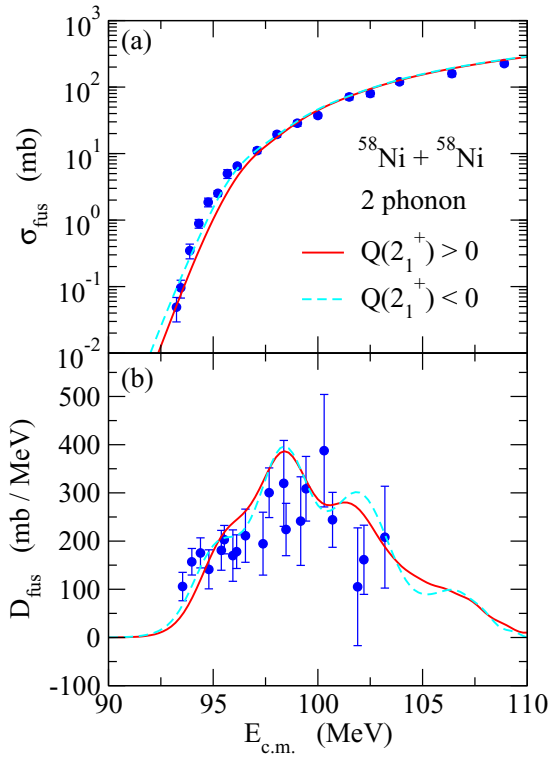

FIG. 7. (Color online) The fusion cross sections (a) and the fusion barrier distributions (b) for the ^{58}Ni + ^{58}Ni system obtained with the MR-CDFT method. The solid line is the same as that in Fig. 4, while the dashed line is obtained by inverting the sign of the quadrupole moment of the first 2^+ state. The experimental data are taken from Refs. [6,44].

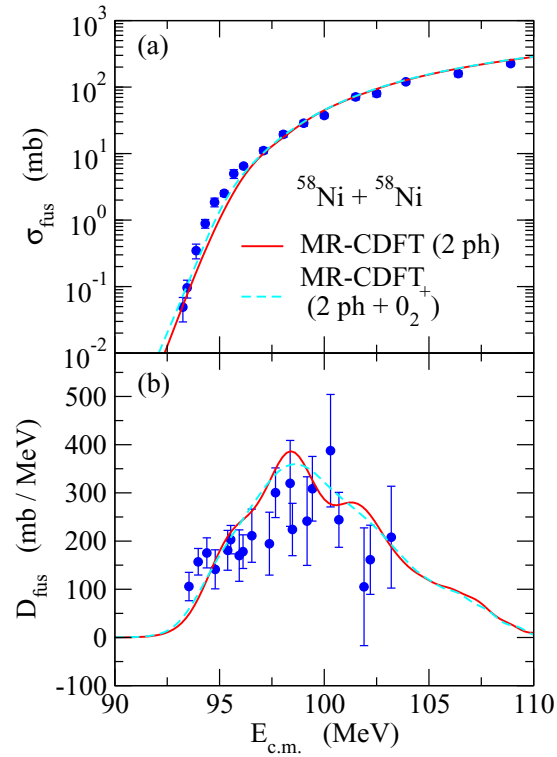

FIG. 8. (Color online) A comparison of the coupled-channels calculations for the ^{58}Ni + ^{58}Ni system with (the dashed line) and without (the solid line) the couplings to the second 0^+ state. Panels (a) and (b) show the fusion cross sections and the fusion barrier distributions, respectively. The experimental data are taken from Refs. [6,44].

solid line is the result with the coupling strengths shown in Table I, while the dashed line is obtained by changing the sign of the quadrupole moment of the first 2^+ state. One can see that the effect of the sign of the quadrupole moment is not large, but is certainly not negligible. Therefore, the conclusion in Refs. [12,13] remains the same; that is, the sign of the quadrupole moment of an excited state can be determined with heavy-ion subbarrier fusion reactions, when high-precision experimental data are available. For the ^{58}Ni + ^{58}Ni system shown in Fig. 7, the experimental data are reproduced slightly better with a negative value of quadrupole moment of the first 2^+ state, which is consistent with the experimental observation [43].

Finally, let us discuss the effect of the second 0^+ state, which couples strongly to the second 2^+ state (see Table I). The dashed line in Fig. 8 is obtained by including the second 0^+ state in the coupled-channels calculations in addition to the two-phonon excitations. However, the solid line shows the result of the two-phonon excitations, which is the same as that in Figs. 4, 6, and 8. Despite the strong coupling between the second 0^+ and the second 2^+ states, one can see that the main feature of the barrier distribution remains the same even when the second 0^+ state is included, although the peak structure is further smeared by the second 0^+ state. This is probably because the second 0^+ state is not directly coupled to the ground state.

Let us next consider the ^{58}Ni + ^{60}Ni reaction, for which high-precision data for fusion cross sections have been measured by Stefanini *et al.* [6]. Table III summarizes the coupling strengths for ^{60}Ni obtained with the MR-CDFT calculations. The main feature of the coupling strengths is similar to that for ^{58}Ni, although the collectivity is somewhat larger in ^{60}Ni than in ^{58}Ni. In particular, strong couplings between the 0_2^+ and 2_2^+ states and between the 0_3^+ and 2_2^+ states remain qualitatively the same. In addition, the reorientation term (that is, the self-coupling term) for the 2_2^+ is much larger in ^{60}Ni as compared to that in ^{58}Ni. Figure 9 shows the results of the coupled-channels calculations with the Woods-Saxon potential with $V_0 = 154.5$ MeV, $r_0 = 1.0$ fm, and $a = 0.9$ fm. Because we would like to compare between the harmonic limit and the MR-CDFT calculations, we consider only the two-phonon couplings, excluding the couplings to the second 0^+ state. Unlike the ^{58}Ni + ^{58}Ni system shown in Fig. 4, the fusion cross sections are largely underestimated at energies below the Coulomb barrier by this calculation. This is probably attributable to the elastic two-neutron transfer process, which is not taken into account in the present coupled-channels calculations, as has been discussed in Ref. [6]. Despite this, however, one may expect that the shape of fusion barrier distribution is not much affected by transfer channels, unless a multinucleon transfer process takes place (which is unlikely

TABLE III. Same as Table I, but for ^{60}Ni.

	I'					
I	0_1^+	2_1^+	0_2^+	2_2^+	4_1^+	0_3^+
0_1^+	0	0.261 (0.288)	0	−0.0101 (−0.0170)	0	0
2_1^+	0.261 (0.288)	−0.0616 (−0.0562)	0.0478 (0.0390)	−0.148 (−0.154)	0.251 (0.267)	0.126 (0.117)
0_2^+	0	0.0478 (0.0390)	0	−0.390 (−0.367)	0	0
2_2^+	−0.0101 (−0.0170)	−0.148 (−0.154)	−0.390 (−0.367)	0.164 (0.151)	−0.0264 (−0.0210)	0.107 (0.114)
4_1^+	0	0.251 (0.267)	0	−0.0264 (−0.0210)	−0.0701 (−0.0681)	0
0_3^+	0	0.126 (0.117)	0	0.107 (0.114)	0	0

in the ^{58}Ni + ^{60}Ni system). The effect of anharmonicity on the shape of fusion barrier distribution is qualitatively the same as that in the ^{58}Ni + ^{58}Ni system. That is, the anharmonicity largely smears the peak structure in the barrier distribution. Even though the agreement with the experimental barrier distribution gets worse by including the anharmonicity effects, it is interesting to notice that the MR-CDFT calculations appear to reproduce the more recent (preliminary) data of the barrier distribution for the same system [47], in a more consistent way than the result of the harmonic approximation.

Last, we briefly discuss the ^{40}Ca + ^{58}Ni fusion reaction. Figure 10 shows the results of the coupled-channels calculations with the Woods-Saxon potential with $V_0 = 135$ MeV, $r_0 = 1.0$ fm, and $a = 0.9$ fm. The excitations up to the two-phonon states are taken into account in the target nucleus ^{58}Ni, while the one-octupole phonon excitation is included for the projectile nucleus, ^{40}Ca, in the harmonic limit. All the mutual excitations are included in the coupled-channels calculation. Because the charge product is small for this system, the inclusion of the second 0^+ state in ^{58}Ni leads to only a marginal change both in the fusion cross sections

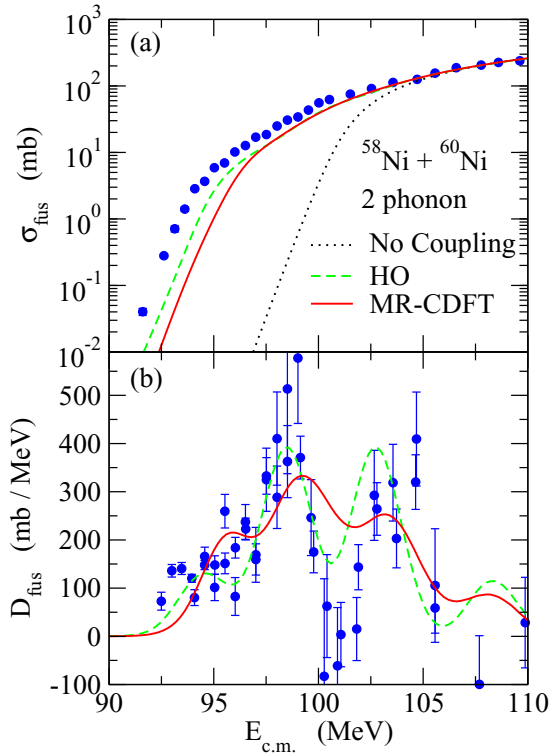

FIG. 9. (Color online) Same as Fig. 4, but for the ^{58}Ni + ^{60}Ni system. The experimental data are taken from Ref. [6].

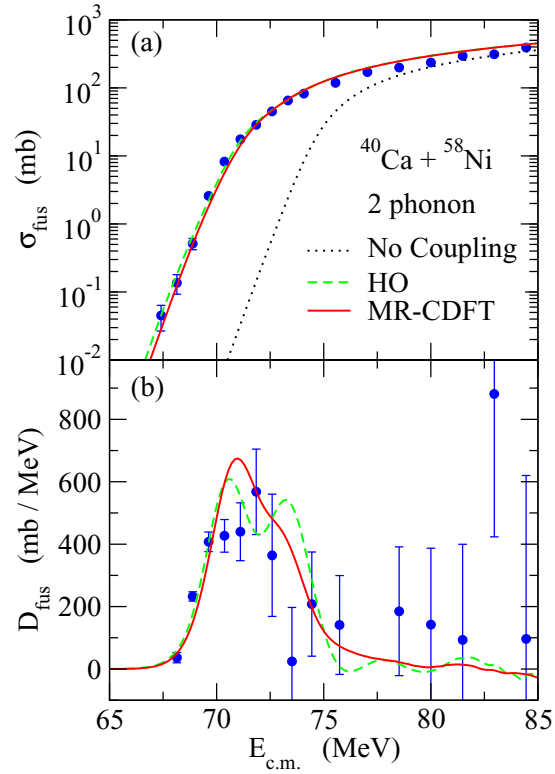

FIG. 10. (Color online) Same as Fig. 4, but for the ^{40}Ca + ^{58}Ni system. The experimental data are taken from Ref. [48].

and in the fusion barrier distribution. Both the harmonic limit and MR-CDFT calculations reproduce well the experimental fusion cross sections [48]. However, in panel (b) of the figure one can again see that the anharmonicity effect in ^{58}Ni smears the fusion barrier distribution, leading to a better agreement with the experimental fusion barrier distribution as compared to the results in the harmonic oscillator limit.

V. SUMMARY

We have proposed a semimicroscopic approach to heavy-ion sub-barrier fusion reactions. The basic idea of this approach is to combine a MR-DFT to a coupled-channels calculation. The MR-DFT provides transition strengths among collective states without resorting to the harmonic oscillator model or the rigid rotor model. It also provides the relative sign for the transition matrix elements. These quantities are usually not known experimentally, and the MR-DFT provides important inputs for the coupled-channels calculations. The excitation energies, however, are often known well, and one can simply use the experimental values for them, although one could use the results of a MR-DFT calculation if the excitation energies are not known experimentally. In this paper, instead of carrying out a fully microscopic calculation for fusion with a double folding potential, we employ the semimicroscopic approach with a phenomenological Woods-Saxon potential, because it has been known that the double folding procedure does not work for subbarrier fusion reactions. The advantages of this approach include that (i) deviations from the harmonic limit as well as the rigid rotor limit can be taken into account, (ii) it can therefore be applied also to transitional nuclei, which show neither the vibrational nor the rotational characters, (iii) the sign of the matrix elements can be determined, (iv) the nuclear coupling strengths can be estimated using the neutron-to-proton ratio for a transition, and (v) a natural truncation is introduced in the coupling schemes.

We have applied this approach to the ^{58}Ni + ^{58}Ni, ^{58}Ni + ^{60}Ni, and ^{40}Ca + ^{58}Ni fusion reactions. We have first discussed the spectrum of ^{58}Ni and ^{60}Ni using the MR-CDFT. We have found that there are both similarities and differences between the calculated spectra and those in the harmonic limit, even though those nuclei have been considered to be typical vibrational nuclei in the literatures. We have then discussed the effect of the anharmonicities on the fusion cross sections and the fusion barrier distributions. We have found that the anharmonicities smear the fusion barrier distributions, somewhat improving the agreement with the experimental data.

In this paper, for simplicity we have assumed the axial and reflection symmetries for the shapes of ^{58}Ni and ^{60}Ni. This has prevented us from including the octupole and the three quadruple-phonon excitations in the coupled-channels calculations. Although the octupole excitations would not affect much the fusion cross sections because the excitation energy is large [5,49], the three quadrupole-phonon excitations may perturb the results presented in this paper. It would be an interesting future problem, even though it may be numerically demanding, to relieve the restriction for the symmetries and repeat the calculations to investigate the role of the three-phonon excitations.

It would also be an interesting problem to extend the treatment presented in this paper to heavy-ion elastic and inelastic scattering. In contrast to fusion reactions, the double-folding approach is applicable to these reactions. One can therefore develop a fully microscopic approach to heavy-ion scattering using the MR-DFT. That approach would also be useful in applications to nuclear data, such as those related to the problem of nuclear transmutation [50].

ACKNOWLEDGMENTS

We thank D. J. Hinde, E. Williams, and A. M. Stefanini for useful discussions on the experimental data. This work was partially supported by the National Natural Science Foundation of China under Grants No. 11305134 and No. 11105111 and the Fundamental Research Funds for the Central University (Grant No. XDJK2013C028).

[1] M. Dasgupta, D. J. Hinde, N. Rowley, and A. M. Stefanini, Annu. Rev. Nucl. Part. Sci. **48**, 401 (1998).
[2] A. B. Balantekin and N. Takigawa, Rev. Mod. Phys. **70**, 77 (1998).
[3] B. B. Back, H. Esbensen, C. L. Jiang, and K. E. Rehm, Rev. Mod. Phys. **86**, 317 (2014).
[4] K. Hagino, N. Rowley, and A. T. Kruppa, Comput. Phys. Commun. **123**, 143 (1999).
[5] K. Hagino and N. Takigawa, Prog. Theor. Phys. **128**, 1061 (2012).
[6] A. M. Stefanini, D. Ackermann, L. Corradi, D. R. Napoli, C. Petrache, P. Spolaore, P. Bednarczyk, H. Q. Zhang, S. Beghini, G. Montagnoli, L. Mueller, F. Scarlassara, G. F. Segato, F. Soramel, and N. Rowley, Phys. Rev. Lett. **74**, 864 (1995).
[7] H. Esbensen, Phys. Rev. C **72**, 054607 (2005).
[8] N. Takigawa and K. Ikeda, in *Proceedings of the Symposium on Many Facets of Heavy-Ion Fusion Reactions*, edited by W. Hennings *et al.*, Report No. ANL-PHY-86-1 (Argonne National Laboratory, Argonne, 1986), p. 613.
[9] A. T. Kruppa, P. Romain, M. A. Nagarajan, and N. Rowley, Nucl. Phys. A **560**, 845 (1993).
[10] J. R. Leigh, M. Dasgupta, D. J. Hinde, J. C. Mein, C. R. Morton, R. C. Lemmon, J. P. Lestone, J. O. Newton, H. Timmers, J. X. Wei, and N. Rowley, Phys. Rev. C **52**, 3151 (1995).
[11] J. M. Yao, M. Bender, and P.-H. Heenen, Phys. Rev. C **91**, 024301 (2015).
[12] K. Hagino, N. Takigawa, and S. Kuyucak, Phys. Rev. Lett. **79**, 2943 (1997).
[13] K. Hagino, S. Kuyucak, and N. Takigawa, Phys. Rev. C **57**, 1349 (1998).
[14] M. Zamrun F. and K. Hagino, Phys. Rev. C **77**, 014606 (2008).
[15] M. Bender, P.-H. Heenen, and P.-G. Reinhard, Rev. Mod. Phys. **75**, 121 (2003).

[16] J. M. Yao, K. Hagino, Z. P. Li, J. Meng, and P. Ring, Phys. Rev. C **89**, 054306 (2014).
[17] T. Furumoto, W. Horiuchi, M. Takashina, Y. Yamamoto, and Y. Sakuragi, Phys. Rev. C **85**, 044607 (2012).
[18] J. O. Newton, R. D. Butt, M. Dasgupta, D. J. Hinde, I. I. Gontchar, C. R. Morton, and K. Hagino, Phys. Lett. B **586**, 219 (2004); Phys. Rev. C **70**, 024605 (2004).
[19] I. I. Gontchar, D. J. Hinde, M. Dasgupta, and J. O. Newton, Phys. Rev. C **69**, 024610 (2004).
[20] K. Hagino, N. Rowley, and M. Dasgupta, Phys. Rev. C **67**, 054603 (2003).
[21] Ei Shwe Zin Thein, N. W. Lwin, and K. Hagino, Phys. Rev. C **85**, 057602 (2012).
[22] A. Mukherjee, D. J. Hinde, M. Dasgupta, K. Hagino, J. O. Newton, and R. D. Butt, Phys. Rev. C **75**, 044608 (2007).
[23] K. Hagino, T. Takehi, A. B. Balantekin, and N. Takigawa, Phys. Rev. C **71**, 044612 (2005).
[24] K. Washiyama, K. Hagino, and M. Dasgupta, Phys. Rev. C **73**, 034607 (2006).
[25] L. R. Gasques, M. Evers, D. J. Hinde, M. Dasgupta, P. R. S. Gomes, R. M. Anjos, M. L. Brown, M. D. Rodriguez, R. G. Thomas, and K. Hagino, Phys. Rev. C **76**, 024612 (2007).
[26] M. Evers, M. Dasgupta, D. J. Hinde, L. R. Gasques, M. L. Brown, R. Rafiei, and R. G. Thomas, Phys. Rev. C **78**, 034614 (2008).
[27] T. Ichikawa, K. Hagino, and A. Iwamoto, Phys. Rev. C **75**, 064612 (2007).
[28] K. Hagino and Y. Watanabe, Phys. Rev. C **76**, 021601 (2007).
[29] T. Ichikawa, K. Hagino, and A. Iwamoto, Phys. Rev. C **75**, 057603 (2007); Phys. Rev. Lett. **103**, 202701 (2009).
[30] T. Ichikawa and K. Matsuyanagi, Phys. Rev. C **88**, 011602(R) (2013).
[31] S. Misicu and H. Esbensen, Phys. Rev. Lett. **96**, 112701 (2006).
[32] P. Ring and P. Schuck, *The Nuclear Many-Body Problem* (Springer-Verlag, Berlin, 1980).
[33] J. M. Yao, J. Meng, P. Ring, and D. Pena Arteaga, Phys. Rev. C **79**, 044312 (2009).
[34] J. M. Yao, J. Meng, P. Ring, and D. Vretenar, Phys. Rev. C **81**, 044311 (2010).
[35] J. M. Yao, H. Mei, and Z. P. Li, Phys. Lett. B **723**, 459 (2013).
[36] M. Zamrun F., Zakarya Mohamed Mohamed Mahmoud, N. Takigawa, and K. Hagino, Phys. Rev. C **81**, 044609 (2010).
[37] P. W. Zhao, Z. P. Li, J. M. Yao, and J. Meng, Phys. Rev. C **82**, 054319 (2010).
[38] National Nuclear Data Center, http://www.nndc.bnl.gov/.
[39] J. M. Allmond, B. A. Brown, A. E. Stuchbery, A. Galindo-Uribarri, E. Padilla-Rodal, D. C. Radford, J. C. Batchelder, M. E. Howard, J. F. Liang, B. Manning, R. L. Varner, and C.-H. Yu, Phys. Rev. C **90**, 034309 (2014).
[40] P. E. Garrett, K. L. Green, and J. L. Wood, Phys. Rev. C **78**, 044307 (2008).
[41] P. E. Garrett and J. L. Wood, J. Phys. G: Nucl. Part. Phys. **37**, 064028 (2010).
[42] W. Greiner and J. Maruhn, *Nuclear Models* (Springer-Verlag, Berlin, 1996).
[43] P. M. S. Lesser, D. Cline, C. Kalbach-Cline, and A. Bahnsen, Nucl. Phys. A **223**, 563 (1974).
[44] M. Beckerman, J. Ball, H. Enge, M. Salomaa, A. Sperduto, S. Gazes, A. Di Rienzo, and J. D. Molitoris, Phys. Rev. C **23**, 1581 (1981).
[45] N. Rowley, G. R. Satchler, and P. H. Stelson, Phys. Lett. B **254**, 25 (1991).
[46] T. Bürvenich, D. G. Madland, J. A. Maruhn, and P.-G. Reinhard, Phys. Rev. C **65**, 044308 (2002).
[47] M. D. Rodriguez, M. L. Brown, M. Dasgupta, D. J. Hinde, D. C. Weisser, T. Kibedi, M. A. Lane, P. J. Cherry, A. G. Muirhead, R. B. Turkentine, N. Lobanov, A. K. Cooper, A. B. Harding, M. Blacksell, and P. M. Davidson, Nucl. Instrum. Methods Phys. Res., Sect. A **614**, 119 (2010); E. Williams (private communications).
[48] D. Bourgin, S. Courtin, F. Haas, A. M. Stefanini, G. Montagnoli, A. Goasduff, D. Montanari, L. Corradi, E. Fioretto, J. Huiming, F. Scarlassara, N. Rowley, S. Szilner, and T. Mijatovic, Phys. Rev. C **90**, 044610 (2014).
[49] N. Takigawa, K. Hagino, M. Abe, and A. B. Balantekin, Phys. Rev. C **49**, 2630 (1994).
[50] E. Sh. Sukhovitskii, Y.-O. Lee, J. Chang, S. Chiba, and O. Iwamoto, Phys. Rev. C **62**, 044605 (2000).